Composite shell formulations: comparison of two geometrically nonlinear implementations

Isadora T. Almeida[1], Celso J. Faccio Junior[1], Alfredo Gay Neto[1], Sergio F. M. Almeida[2]

[1]*Dept. of Structural and Geotechnical Engineering, University of São Paulo*
Av. Prof. Almeida Prado, Tv. 2, 83, 05508-070, São Paulo/SP, Brazil
isadora.toledo.almeida@usp.br, celsojf@usp.br, alfredo.gay@usp.br
[2]*Dept. of Mechatronic and Mechanical Systems, University of São Paulo*
Av. Prof. Mello Moraes, 2231, 05508-030, São Paulo/SP, Brazil
sergio.frascino@usp.br

Abstract. Composite materials are attractive candidates for structural applications that require high specific-strength and high specific-stiffness. Laminated composite materials are extensively used in aeronautical, aerospace, and lately wind energy industries, where weight-sensitive structures are abundant. The structural modeling of laminates commonly employs the Classical Lamination Theory (CLT). It is an extension of the homogeneous plate theory introducing the elastic coupling effects present in laminates. In the CLT, the laminate stacking sequence and material properties of each layer generate a homogenized section. Also, these structures are often slender and may present large displacements and finite rotations, so that the adoption of a geometrically nonlinear shell model is appropriate. This work presents the extension of a fully geometrically nonlinear triangular shell finite element to account for laminated composite materials. The constitutive relations are derived from a quadratic potential based on the CLT, considering small strains. The method was implemented in the Giraffe solver, accounting for transverse shear and an additional drilling stiffness parameter. Calibration of the drilling stiffness was performed by comparing static results from ANSYS® software, as a reference. Modal analysis was also addressed, for the same composite proposals. Numerical results showed good agreement between Giraffe and ANSYS® implementations.

Keywords: composite shells, CLT, nonlinear shell formulation

1 Introduction

Fiber-reinforced composite (FRC) materials take advantage of both stiff, resistant fibers and ductile, resilient matrix to exhibit the best structural qualities of their constituents. Composite laminates are a bonded stack of FRC layers with multiple orientations. Lamination enables the tailoring of the material to prescribed structural requirements with little waste of material capability, as described by Jones [1]. Therefore, composite laminates are a cost-effective alternative for structural applications that are weight-sensitive, such as aeronautical, aerospace, and wind energy.

Optimal tailoring of the material to meet the structural requirements depends on choosing a reliable model concerning its constitutive relations. As lightweight is generally the main design guideline in these structures, the model must be able to cope with structural slenderness, which commonly is accompanied by geometric non-linearities, such as large deformations and finite rotations. The Classical Lamination Theory (CLT) qualifies for describing the stress-strain relations and has been widely used in laminate structural modeling. It extends the homogeneous plate theory based on the orthotropic layer assumption to enable the determination of the laminate stress state. In the CLT, the laminate stacking sequence and the material properties of each layer generate a plate section. Assuming a through-thickness continuous displacement field, the intrinsically compound nature of the laminate leads to a discontinuous stress field in the plate model and the bonded interface, consequently, to elastic coupling effects.

As previously mentioned, the structural slenderness commonly leads to geometric nonlinear scenarios, requiring a nonlinear framework. Therefore, a fully nonlinear geometrically exact shell model with a standard

Reissner-Mindlin kinematical assumption is eligible, as proposed by Simo and Fox [2], Campello et al. [3], and others. On the other hand, the CLT constitutive relations can be derived, under small strains, from a quadratic potential.

This work presents the extension of the finite element shell formulation of Campello et al. [3], and Ota et al. [4] to include laminated composite materials in the finite element solver Giraffe implementation [5]. The implementation is verified by a comparative assessment of numerical results with the ANSYS® solver.

2 Shell model

2.1 Kinematics

The shell model refers to the updated-Lagrangian description used by Ota et al. [4] and based on Campello et al. [3],[6]. In the updated model, three configurations are described by local orthonormal frames, as in Fig. 1: $\{\boldsymbol{e}_1^r, \boldsymbol{e}_2^r, \boldsymbol{e}_3^r\}$ as the assumed-plane initial reference configuration Ω^r, $\{\boldsymbol{e}_1^i, \boldsymbol{e}_2^i, \boldsymbol{e}_3^i\}$ the configuration at instant "i", Ω^i, and $\{\boldsymbol{e}_1^{i+1}, \boldsymbol{e}_2^{i+1}, \boldsymbol{e}_3^{i+1}\}$ the configuration at instant "$i+1$", Ω^{i+1}.

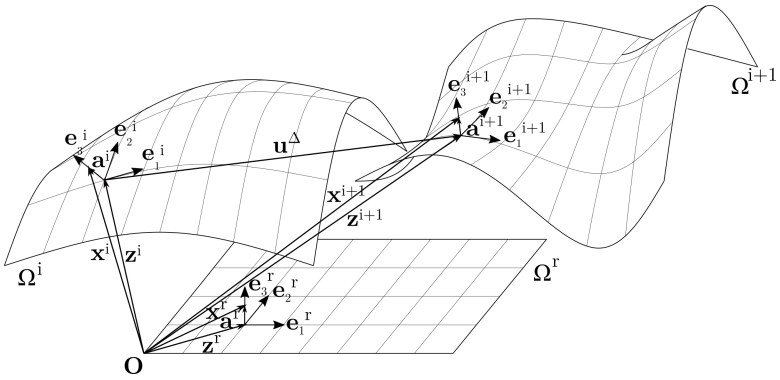

Figure 1. Updated shell model: instants and configurations

The quantities are back-rotated to the reference configuration to avoid non-objectivity due to rigid body motion. The deformation, summarized at the instant "$i+1$" by the tensor $\boldsymbol{Q}^{i+1}$, can be described in an incremental manner. The rotation tensor $\boldsymbol{Q}^{\Delta}$ updates the position vector fields from the instant"i" to "$i+1$", namely $\boldsymbol{x}^i$ to $\boldsymbol{x}^{i+1}$, and $\boldsymbol{Q}$ describes the accumulated transformation until the instant "i", relating $\boldsymbol{x}^r$ and $\boldsymbol{x}^i$, as shown in eq. (1).

$$\boldsymbol{x}^{i+1} = \boldsymbol{Q}^{\Delta}\boldsymbol{Q}\boldsymbol{x}^r = \boldsymbol{Q}^{i+1}\boldsymbol{x}^r. \tag{1}$$

In the reference configuration, the position of any material point in the shell domain can be completely described by the mid-surface position $\boldsymbol{z}^r$ and the shell director $\boldsymbol{a}^r = \zeta \boldsymbol{e}_3^r$, so that $\zeta \in H = [-h^b, h^t]$ is the depth coordinate with respect to the reference mid-surface and the shell thickness $h = h^b + h^t$. The application of eq. (1) to the shell director not only implies its inextensibility, but also ensures the Reissner-Mindlin kinematical constraint, since fibers initially aligned with the shell director remain aligned with it at any further configuration, as $\boldsymbol{a}^{i+1} = \zeta \boldsymbol{e}_3^{i+1}$.

The shell back-rotated cross-sectional strain vectors at the instant "$i+1$" can be defined as follows:

$$\boldsymbol{\eta}_{\alpha}^{i+1^r} = \boldsymbol{Q}^{i+1^T}\boldsymbol{z}_{,\alpha}^{i+1} - \boldsymbol{e}_{\alpha}^r, \;\; \boldsymbol{\kappa}_{\alpha}^{i+1^r} = axial\left(\boldsymbol{Q}_{,\alpha}^{i+1}\boldsymbol{Q}^{i+1^T}\right), \tag{2}$$

where $\boldsymbol{\eta}_{\alpha}^{i+1^r}$ is the translational strain vector, and $\boldsymbol{\kappa}_{\alpha}^{i+1^r}$, the specific rotation vector.

Remark 1: Notation. In the text, the greek indices range from 1 to 2, referring to in-plane quantities. Besides, summation convention over repeated indices is adopted.

2.2 Statics

As an updated, pure-displacement based formulation, the internal and external loads power are related to the incremental displacement field $\boldsymbol{d}^{\Delta}$. Therefore, the stress power at the instant "$i+1$", computed in the plane reference shell domain Ω^r, may be written as:

$$P_{int}^{i+1} = \int_{\Omega^r} \boldsymbol{\sigma}_{\alpha}^{i+1^r} \cdot \dot{\boldsymbol{\varepsilon}}_{\alpha}^{i+1^r} d\Omega^r, \tag{3}$$

where $\boldsymbol{\sigma}_{\alpha}^{i+1^r}$ and $\dot{\boldsymbol{\varepsilon}}_{\alpha}^{i+1^r}$ respectively summarize the cross-sectional stress and strain-rate vectors:

$$\boldsymbol{\sigma}_{\alpha}^{i+1^r} = \begin{bmatrix} \boldsymbol{n}_{\alpha}^{i+1^r} \\ \boldsymbol{m}_{\alpha}^{i+1^r} \end{bmatrix}, \;\; \dot{\boldsymbol{\varepsilon}}_{\alpha}^{i+1^r} = \begin{bmatrix} \dot{\boldsymbol{\eta}}_{\alpha}^{i+1^r} \\ \dot{\boldsymbol{\kappa}}_{\alpha}^{i+1^r} \end{bmatrix} = \boldsymbol{\Psi}_{\alpha} \dot{\boldsymbol{d}}^{\Delta}, \tag{4}$$

in which $\boldsymbol{n}_{\alpha}^{i+1^r}$ and $\boldsymbol{m}_{\alpha}^{i+1^r}$ are the back-rotated cross-sectional forces and moments per unit length. The operator $\boldsymbol{\Psi}_{\alpha}$ is fully described in [3]. These forces and moments are obtained from the standard definition, as shown in eq. (5):

$$\boldsymbol{n}_{\alpha}^{i+1^r} = \int_H \boldsymbol{\tau}_{\alpha}^{i+1^r} d\zeta, \;\; \boldsymbol{m}_{\alpha}^{i+1^r} = \int_H \boldsymbol{a}^{i+1^r} \times \boldsymbol{\tau}_{\alpha}^{i+1^r} d\zeta, \;\; \boldsymbol{d}^{\Delta} = \begin{bmatrix} \boldsymbol{u}^{\Delta} \\ \boldsymbol{\alpha}^{\Delta} \end{bmatrix}, \tag{5}$$

where $\boldsymbol{\tau}_{\alpha}^{i+1^r}$ are the back-rotated stress vectors, and $\boldsymbol{u}^{\Delta}$ and $\boldsymbol{\alpha}^{\Delta}$ the translational and rotational incremental displacement fields.

The shell external power at instant "$i+1$" is given by:

$$P_{ext}^{i+1} = \int_{\Omega^r} \bar{\boldsymbol{q}} \cdot \dot{\boldsymbol{d}}^{\Delta} d\Omega^r, \tag{6}$$

with $\bar{\boldsymbol{q}}$ as the generalized external forces vector per unit area of the mid-surface in the reference configuration.

The weak form is obtained from the virtual work theorem, and its linearization leads to the tangent bilinear form in the shell domain Ω^r:

$$\delta^*(\delta W) = \int_{\boldsymbol{\Omega^r}} \delta \boldsymbol{d}^T \boldsymbol{\Psi}_{\alpha}^T \bar{\boldsymbol{D}}_{\alpha\beta} \boldsymbol{\Psi}_{\beta} \delta^* \boldsymbol{d} \, d\Omega^r + \int_{\boldsymbol{\Omega^r}} \delta \boldsymbol{d}^T \boldsymbol{\Delta}_{\alpha}^T \boldsymbol{G}_{\alpha} \boldsymbol{\Delta}_{\alpha} \delta^* \boldsymbol{d} \, d\Omega^r \; - \; \int_{\boldsymbol{\Omega^r}} \delta^T \boldsymbol{L} \delta^* \boldsymbol{d} \, d\Omega^r, \tag{7}$$

where the symbol δ stands for virtual quantities, and δ^*, for the linearized quantitities with respect to $\boldsymbol{d}^{\Delta}$. The matrices $\bar{\boldsymbol{D}}$ and $\boldsymbol{G}$ are the generalized constitutive and geometric tangent stiffnesses, and $\boldsymbol{L}$ is the external load geometric tangent stiffness (zero, when no follower loads are considered).

2.3 CLT constitutive relations

The CLT constitutive relations derive from the assumption of a linear elastic quadratic potential:

$$\boldsymbol{\Psi}(\boldsymbol{\varepsilon}^{i+1^r}) = \frac{1}{2} \boldsymbol{\varepsilon}^{i+1^r} \cdot \bar{\boldsymbol{D}} \boldsymbol{\varepsilon}^{i+1^r} = \frac{1}{2} \boldsymbol{\varepsilon}_{\alpha}^{i+1^r} \cdot \bar{\boldsymbol{D}}_{\alpha\beta} \boldsymbol{\varepsilon}_{\beta}^{i+1^r}, \tag{8}$$

where the cross-sectional generalized stresses and strains are related by the generalized constitutive tangent stiffness matrix, $\bar{\boldsymbol{D}}$, given by its sub-matrices $\bar{\boldsymbol{D}}_{\alpha\beta}$ as follows:

$$\bar{\boldsymbol{D}}_{\alpha\beta} = \frac{\partial \boldsymbol{\sigma}_{\alpha}^{i+1^r}}{\partial \boldsymbol{\varepsilon}_{\beta}^{i+1^r}} = \begin{bmatrix} \frac{\partial \boldsymbol{n}_{\alpha}^{i+1^r}}{\partial \boldsymbol{\eta}_{\beta}^{i+1^r}} & \frac{\partial \boldsymbol{n}_{\alpha}^{i+1^r}}{\partial \boldsymbol{\kappa}_{\beta}^{i+1^r}} \\ \frac{\partial \boldsymbol{m}_{\alpha}^{i+1^r}}{\partial \boldsymbol{\eta}_{\beta}^{i+1^r}} & \frac{\partial \boldsymbol{m}_{\alpha}^{i+1^r}}{\partial \boldsymbol{\kappa}_{\beta}^{i+1^r}} \end{bmatrix}, \tag{9}$$

so that the $\bar{\boldsymbol{D}}$ matrix corresponds to the CLT well-known $\boldsymbol{ABD}$ matrix.

$$\begin{bmatrix} \boldsymbol{n}^r \\ \boldsymbol{m}^r \end{bmatrix} = \begin{bmatrix} \boldsymbol{A} & \boldsymbol{B} \\ \boldsymbol{B} & \boldsymbol{D} \end{bmatrix} \begin{bmatrix} \boldsymbol{\eta}^r \\ \boldsymbol{\kappa}^r \end{bmatrix}, \tag{10}$$

where the sub-matrices $\boldsymbol{A}$, $\boldsymbol{B}$, and $\boldsymbol{D}$ are extensional, coupling and flexural stiffnessess, as given:

$$\boldsymbol{A} = \sum_k (h_k - h_{k-1}) \bar{\boldsymbol{Q}}_{p_k}, \tag{11}$$

$$\boldsymbol{B} = \sum_k \frac{(h_k^2 - h_{k-1}^2)}{2} \bar{\boldsymbol{Q}}_{p_k}, \tag{12}$$

$$\boldsymbol{D} = \sum_k \frac{(h_k^3 - h_{k-1}^3)}{3} \bar{\boldsymbol{Q}}_{p_k}, \tag{13}$$

in which $\bar{\boldsymbol{Q}}_{p_k}$ and $\bar{\boldsymbol{Q}}_{t_k}$ are the material tangent moduli at the k^{th} layer, where the subscript p refers to the membrane quantities derived from the plane stress assumption, and t, transverse quantities. Both moduli are defined in the laminate global coordinate system so that their contributions can be summed up to a homogenized section.

Remark 2: Transverse shear and drilling DOF. The CLT was originally developed on a Kirchhoff plate theory context so that we must adapt the relations above to account for transverse shear in a Reissner-Mindlin fashion. Also, the extension to a shell model requires an additional drilling degree of freedom, which must belong to the constitutive relations. The additional relations adopt the matrices from eq. (14) and eq. (15), retrieved from Chróścielewski et al. [7].

$$\boldsymbol{S} = \alpha_s \sum_k (h_k - h_{k-1}) \bar{\boldsymbol{Q}}_{t_k}, \tag{14}$$

$$\boldsymbol{G} = \alpha_t \sum_k \frac{(h_k^3 - h_{k-1}^3)}{3} \bar{\boldsymbol{Q}}_{t_k}, \tag{15}$$

in which $\boldsymbol{S}$ represents the transverse shear stiffnesses, and $\boldsymbol{G}$, the drilling couples. The shear correction factor $\alpha_s = \frac{5}{6}$ is applied to the through-thickness uniform shear strain (and stresses), and α_t is a numeric factor that will be calibrated in next section.

Remark 3: Modal analysis. The last numerical example of Section (3) is a modal analysis. For a correct description of the model, one must account for the mass distribution, as shown in eq. (16). The mass matrix itself can be obtained by applying this distribution in the finite element interpolation procedure described in [3].

$$\boldsymbol{M} = \sum_k \int_{\Omega^r} \int_{h_{k-1}}^{h_{k+1}} \rho_k \, d\zeta d\Omega^r, \tag{16}$$

where ρ_k is the specific mass of the composite material at each layer.

3 Results

The following numerical examples assess the formulation herein presented by comparing the results with the commercial finite element code ANSYS®, as a reference. The examples were adapted from Barbero [8], comprising different laminate stacking sequences (LSS), from unidirectional (UD), to symmetric, and asymmetric laminates. All plates were laminated with carbon/epoxy AS4D/9310, with the following material properties:

Table 1. Material properties of UD carbon/epoxy AS4D/9310

Property	Value
E_1	133.86 GPa
$E_2 = E_3$	7.706 GPa
$G_{12} = G_{13}$	4.306 GPa
G_{23}	2.76 GPa
$\nu_{12} = \nu_{13}$	0.301
ν_{12}	0.396
ρ	1.52 g/cm³

3.1 UD laminate: simply supported, transversely loaded rectangular plate

A simply supported rectangular plate, $a_x = 4000\ mm$, $a_y = 2000\ mm$, thickness $t = 10\ mm$ is transversely loaded by a uniform pressure $q_0 = 0.12 \times 10^{-3}\ MPa$, as represented in Fig. 2. The laminate is unidirectional, with the fibers oriented in the x direction. Vertical displacements obtained for the center point of the plate were compared for geometrically nonlinear simulations in both software. Figure 3 overlays almost coincident curves, showing good agreement even for a coarse mesh.

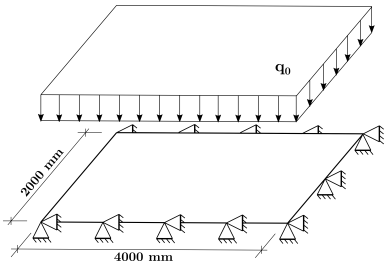

Figure 2. Problem definition for example 3.1

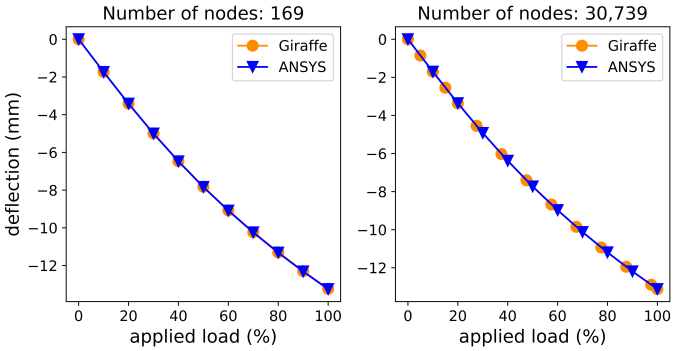

Figure 3. Center point deflection results for ANSYS® and Giraffe for two refinement standards

Remark 4: Drilling calibration. The simulation results for this example were almost identical for the adopted α_t numerical factor range of calibration so that the results for $\alpha_t = 1$ were considered.

3.2 $[0/90]_n$ configuration laminate: simply supported, axially loaded square plate

Figure 4 shows a simply supported square plate, $a_x = a_y = 2000\ mm$, and thickness $t = 10\ mm$ loaded in compression with an edge load $N_x = -1\ N/mm$. The laminate is a crossply $[0/90]_n$ and Fig. 5 depicts the plate center point vertical displacement for $n = 1, 10, 20$. As the plate is axially loaded, the deflection at its

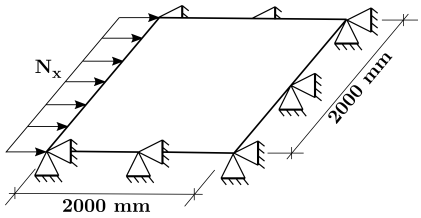

Figure 4. Problem definition for example 3.2

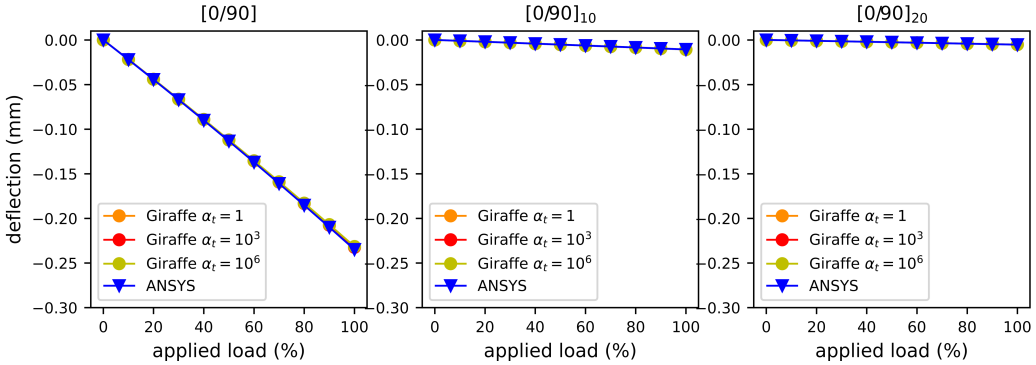

Figure 5. Center point deflection results for ANSYS® and Giraffe (results for 485 nodes)

center is a coupling displacement. It is clear from Fig. 3 that its value reduces drastically with the increase of homogeneity in the laminate stacking sequence. Also, the results were computed for $\alpha_t = \{1, 10^3, 10^6\}$, and no relevant differences were observed so that $\alpha_t = 1$ was fixed.

3.3 Prestressed modal analysis

This last example was performed to assess the model's robustness in a prestressed modal analysis. The laminate adopted was a $[0/90]$, loaded in compression as in Example 3.2. Figure 6 shows the natural frequencies to the first twelve modes obtained from both software frameworks, and Fig. 7 the first three mode shapes.

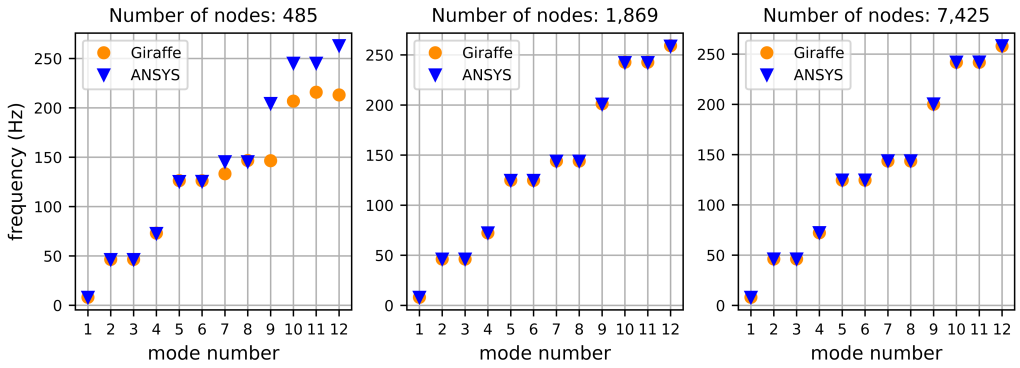

Figure 6. First twelve natural frequencies for three simulations with increasing refinement

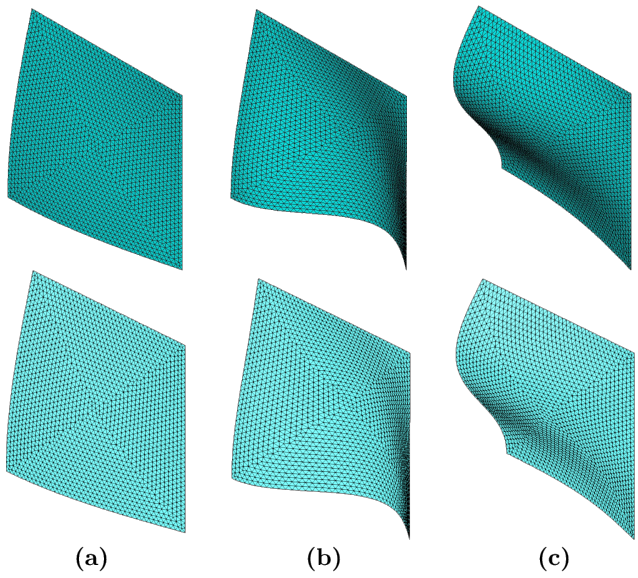

Figure 7. First (a), second (b), and third (c) mode shapes for Giraffe (top) and ANSYS® (bottom)

Remark 5: Symmetry fixture. All simulations in this work were carried out with a $\frac{1}{4}$ of plate model, considering the symmetry in the xz and yz planes, including the modal analyses. Although this modeling strategy suits well for numerical benchmark purposes, one must avoid this assumption in real structural modeling, for the symmetry boundary conditions may disable capturing skew modes.

4 Conclusions

This work presented the extension of a geometrically exact shell model to laminated composite materials, based on the CLT. A comparative assessment of the numerical results was conducted, demonstrating very good agreement between Giraffe and ANSYS® implementations. The numeric factor related to the drilling degree of freedom showed little influence in the results, so that any value in the range $]0, 10^6]$ can be adopted.

Acknowledgements. The first author acknowledges Petróleo Brasileiro S.A. - Petrobras for the support through the Deep Waters Offshore Floating Wind Turbine (DWOFWT) Chair project. The third author acknowledges the National Council for Scientific and Technological Development (CNPq) under the grant 304680/2018-4.

Authorship statement. The authors hereby confirm that they are the sole liable persons responsible for the authorship of this work, and that all material that has been herein included as part of the present paper is either the property (and authorship) of the authors, or has the permission of the owners to be included here.

References

[1] R. M. Jones. *Mechanics of Composite Materials*. CRC Press, 2018.
[2] J. Simo and D. Fox. On a stress resultant geometrically exact shell model. part i: Formulation and optimal parametrization. *Computer Methods in Applied Mechanics and Engineering*, vol. 72, 1989.
[3] E. M. B. Campello, P. M. Pimenta, and P. Wriggers. A triangular finite shell element based on a fully nonlinear shell formulation. *Computational Mechanics*, vol. 31, 2003.
[4] N. Ota, L. Wilson, A. G. Neto, S. Pellegrino, and P. Pimenta. Nonlinear dynamic analysis of creased shells. *Finite Elements in Analysis and Design*, vol. 121, 2016.
[5] A. G. Neto. Giraffe, 2021.
[6] E. M. B. Campello. Modelos não-lineares de casca em elasticidade e elastoplasticidade com grandes deformações: teoria e implementação em elementos finitos, 2005.
[7] J. Chróścielewski, I. Kreja, A. Sabik, and W. Witkowski. Modeling of composite shells in 6–parameter nonlinear theory with drilling degree of freedom. *Mechanics of Advanced Materials and Structures*, vol. 18, 2011.
[8] E. J. Barbero. *Finite Element Analysis of Composite Materials Using Ansys®*. CRC Press, 2 edition, 2014.